JOURNAL OF MAGNETIC RESONANCE 75, 474–492 (1987)

Practical Aspects of the E.COSY Technique. Measurement of Scalar Spin–Spin Coupling Constants in Peptides

C. GRIESINGER, O. W. SØRENSEN, AND R. R. ERNST

Laboratorium für Physikalische Chemie, Eidgenössische Technische Hochschule, 8092 Zurich, Switzerland

Received April 12, 1987

Practical aspects of the E.COSY technique for measurement of coupling constants are discussed. Guidelines are presented for the experimental setup and for spectral assignments. The features of E.COSY cross-peak multiplet patterns are illustrated by experimental spectra of valine, phenylalanine, and proline residues in the decapeptide antamanide. © 1987 Academic Press, Inc.

INTRODUCTION

In conformational studies of molecules by NMR, it is desirable to accurately measure scalar coupling constants as their magnitudes and signs are closely related to the molecular conformation, for example in terms of dihedral angles (*1–3*).

For small molecules, J values can be determined from standard one-dimensional spectra, either by direct measurement of multiplet splittings or, for strongly coupled spin systems, by computer simulation and fit procedures. On the other hand, for unraveling the spectra of large molecules such as peptides, proteins, and nucleic acids, two-dimensional NMR techniques (*4*) are indispensable (*5*).

In the early days of 2D NMR spectroscopy the (J, δ) 2D separation experiment (*6, 7*) was employed for measurement of J. This experiment suffers, however, from drawbacks such as phase-twisted peakshapes and artifacts in the case of strong coupling. Multiplets with identical chemical shifts cannot be resolved due to the lack of chemical-shift dispersion in the ω_1 frequency dimension. These drawbacks are largely absent in 2D *co*rrelation *s*pectroscop*y* (COSY) (*8, 9*) and in its multiple-quantum-filtered variants (*10–12*). Nevertheless, coupling constants can be extracted directly only for sufficiently simple and fully resolved cross-peak multiplet patterns (*13*). Some improvement toward the analysis of more complex patterns was provided by the DISCO procedure of Oschkinat *et al.* (*14, 15*) which involves linear combinations of different cross peaks in a COSY spectrum.

In this paper we demonstrate that the simplified cross-peak multiplet patterns obtained in *ex*clusive *co*rrelation *s*pectroscop*y* (E.COSY) (*16, 17*) exhibit ideal features for measurement and assignment of coupling constants. In addition, practical aspects are discussed, such as the selection of scan numbers. A sensitivity comparison for the E.COSY variants is also given.

0022-2364/87 $3.00

THEORETICAL BACKGROUND

This section briefly summarizes the results of the general treatment presented in Ref. (*17*). E.COSY employs the three-pulse sequence shown in Fig. 1. It is identical to the sequence used for multiple-quantum-filtered (MQF) COSY. In the limit of weak coupling, coherence transfer by the two mixing pulses $(\pi/2)_\beta$ and $(\pi/2)_\pi$ is restricted to take place exclusively between connected transitions in the energy level diagram. This is equivalent to the statement that no passive spins change their spin states during the mixing process. The implications for cross-peak multiplets are discussed in detail in the next section.

The result of an E.COSY experiment can be understood as a linear combination of MQF COSY spectra of different orders,

$$\{\text{E.COSY}\} = \sum_{p=0}^{K} B_p\{p\text{QF}\}. \qquad [1]$$

The weight factors B_p for the MQ orders p are, conveniently normalized, given by

$$B_p = \tfrac{1}{4}p^2 + B_0, \qquad \text{for } p \text{ even}, \qquad [1a]$$

$$B_p = \tfrac{1}{4}(p^2 - 1) + B_1, \qquad \text{for } p \text{ odd}. \qquad [1b]$$

The weights of the zero- and single-quantum-filtered spectra, B_0 and B_1, respectively, are free parameters. Usually they are both set to zero since this selection results in the most attractive diagonal peak characteristics (no net magnetization). The highest order K to be included in the linear combination is determined by the cross-peak selection rule of MQF COSY spectra (*10*). For a given cross peak, the order K must be included only if the cross peak would appear in the KQF COSY spectrum, i.e., if the two spins between which the cross peak occurs possess at least $K-2$ common coupling partners.

The principles of the E.COSY technique can be illustrated with a three-spin system. For $B_0 = B_1 = 0$ we obtain from Eqs. [1a] and [1b] $B_2 = 1$ and $B_3 = 2$, respectively. An experimental E.COSY spectrum of 2,3-dibromopropionic acid is shown at the top of Fig. 2. Also shown, on an expanded scale, is the framed cross-peak multiplet as it appears in 2QF COSY, 3QF COSY, E.COSY, and complementary E.COSY spectra. The phase cycles for 2QF and 3QF COSY spectra (see the legend to Fig. 1) employed four and six scans, respectively, and the E.COSY linear combination according to Eq. [1] is $\{\text{E.COSY}\} = \{2\text{QF}\} + \frac{4}{6}\cdot 2\{3\text{QF}\}$. The subtractive combination with the same weights leads to the complementary E.COSY spectrum correlating anticonnected

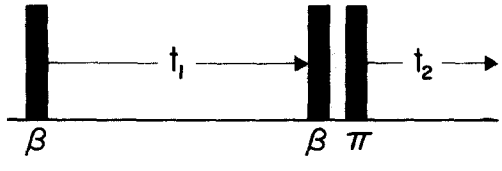

FIG. 1. Pulse sequence for multiple-quantum-filtered COSY and E.COSY consisting of three 90° pulses. In p-quantum filtered COSY the phase β is cycled through the values $j(\pi/p)$, $k = 0, 1, \ldots, 2p-1$, with alternate addition and subtraction of the FIDs. The phase of the third pulse is fixed and equal to π or $-x$. The phase cycle for β in E.COSY experiments is given in the text.

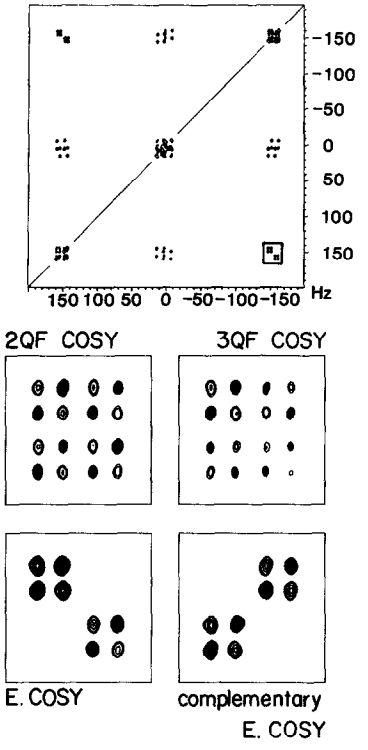

FIG. 2. Top: E.COSY survey spectrum of 2,3-dibromopropionic acid dissolved in benzene-d_6. The framed cross peak is plotted on expanded scale for 2QF COSY, 3QF COSY, E.COSY, and complementary E.COSY spectra. Intensity distortions by strong coupling are observed, especially in the 3QF COSY excerpt. The contours are drawn at 85.5, 68.4, 51.3, 34.1, and 25.6% of the highest peak intensity in the E.COSY excerpt with filled contours for negative peaks.

transitions. In general, complementary E.COSY requires a sign change of B_p for all odd values of p:

$$B_p^{\text{comp.}} = (-1)^p B_p. \qquad [2]$$

The entire set of weights B_p of Eqs. [1a] and [1b] forms a multiple-quantum weighting function $\{B_p\}$ that is illustrated in Fig. 3 for $B_0 = B_1 = 0$. Because all MQF COSY spectra employ the same pulse sequence, it is possible to convert such a multiple-quantum weighting function into a unique cycle for the phase β. The selection of K-quantum coherence can be achieved with a $2N$-step phase cycle with $N \geqslant K$:

$$\beta_j = j\frac{\pi}{N}, \qquad j = 0, 1, 2, \ldots, 2N-1. \qquad [3]$$

The weight factor W_j for the spectrum recorded with phase β_j is obtained by Fourier transformation of the multiple-quantum weighting function $\{B_p\}$ (*17*):

$$W_j = \tfrac{1}{2}B_0 + \sum_{p=1}^{K} B_p \cos(p\beta_j) - \tfrac{1}{2}\delta_{N,K} \cdot B_K \cos(K\beta_j). \qquad [4]$$

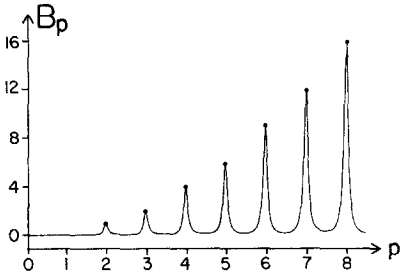

FIG. 3. E.COSY multiple-quantum weighting function with $B_0 = B_1 = 0$. Only integer values of p occur, and there is no significance to the width of the "lines."

The resulting phase cycles for the two cases $N = K = 3$ and $N = K = 4$ are given in Table 1, both for the assumption $B_0 = B_1 = 0$.

The weights $W_j^{\text{comp.}}$ for complementary E.COSY are related to those of normal E.COSY (*17*) by

$$W_j^{\text{comp.}} = W_{j+N}. \qquad [5]$$

THE STRUCTURE OF E.COSY CROSS-PEAK MULTIPLETS

The basic pattern in E.COSY spectra can be understood by starting with the energy level diagram of a two-spin system I_1–I_2. Both transitions of one spin are connected to both transitions of the other spin leading to four-line cross-peak multiplets in the 2D spectrum. The four components are arranged as a $\begin{pmatrix} + & - \\ - & + \end{pmatrix}$ square with peak separation J_{12} along ω_1 and ω_2. The J coupling giving rise to a cross peak is called the active coupling for that particular cross peak.

TABLE 1

Weights W_j of the Individual Phase-Shifted Experiments in Normal and Complementary E.COSY for $N = K = 3,4$

$N = K = 3$								
β_j (E.COSY)	0°	60°	120°	180°	240°	300°		
W_j	2	$-\frac{3}{2}$	$\frac{1}{2}$	0	$\frac{1}{2}$	$-\frac{3}{2}$		
	(4)	(−3)	(1)	(0)	(1)	(−3)		
β_j (comp. E.COSY)	180°	240°	300°	0°	60°	120°		
$N = K = 4$								
β_j (E.COSY)	0°	45°	90°	135°	180°	225°	270°	315°
W_j	5	$-2-\sqrt{2}$	1	$-2+\sqrt{2}$	1	$-2+\sqrt{2}$	1	$-2-\sqrt{2}$
	(10)	(−7)	(2)	(−1)	(2)	(−1)	(2)	(−7)
β_j (comp. E.COSY)	180°	225°	270°	315°	0°	45°	90°	135°

Note. In parentheses are recommended numbers of scans for the phase-shifted experiments which can be combined directly without numerical scaling. These are exact for $K = 3$ and approximate for $K = 4$.

Further spins coupled to the two active spins are referred to as passive spins. The couplings between active and passive spins are called passive couplings. Because passive spins are "unperturbed" by the mixing process in E.COSY, the cross-peak multiplets for larger spin systems can be imagined as arising from a superposition of displaced two-spin multiplets, i.e., $\left(\begin{smallmatrix}+&-\\-&+\end{smallmatrix}\right)$ square patterns. The number of squares contained in a cross-peak multiplet is 2^{K-2} for K mutually coupled spins, i.e., equal to the number of possible spin polarizations of the $K-2$ passive spins.

For example, four squares occur in the $I_1 \rightarrow I_2$ cross peak of an I_1–I_2–I_3–I_4 spin system with the centers of the squares at the frequencies

$$\{\nu_1 + \tfrac{1}{2}(J_{13}+J_{14}), \nu_2 + \tfrac{1}{2}(J_{23}+J_{24})\}, \qquad \{\nu_1 + \tfrac{1}{2}(J_{13}-J_{14}), \nu_2 + \tfrac{1}{2}(J_{23}-J_{24})\},$$

$$\{\nu_1 - \tfrac{1}{2}(J_{13}-J_{14}), \nu_2 - \tfrac{1}{2}(J_{23}-J_{24})\}, \qquad \{\nu_1 - \tfrac{1}{2}(J_{13}+J_{14}), \nu_2 - \tfrac{1}{2}(J_{23}+J_{24})\}.$$

Note that the signs in front of J_{1i} and J_{2i} in ω_1 and ω_2, respectively, must be identical. In normal or in double-quantum-filtered COSY this restriction does not apply and a total of $2^{2(K-2)}$ square patterns results.

Typical E.COSY cross-peak multiplet patterns for three- and four-spin systems are illustrated in Fig. 4. Two types of vectors are relevant for measurement of J. The displacement vectors, represented by arrows with solid lines, are associated with a specific passive spin I_i and have the components $(\omega_1, \omega_2) = (J_{1i}, J_{2i})$. A displacement vector always connects peaks of like signs. The angle φ_i between the ω_2 axis and the

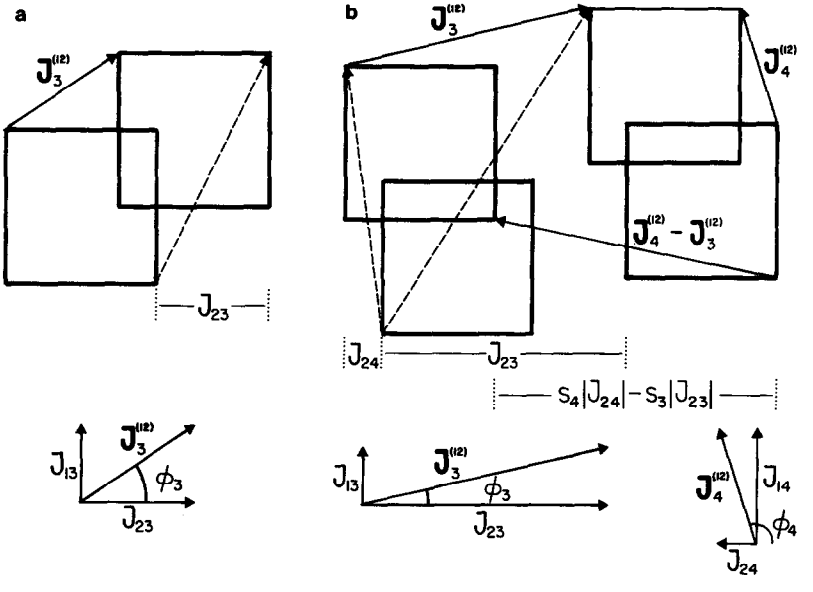

FIG. 4. $I_1 \rightarrow I_2$ E.COSY cross-peak multiplet patterns for (a) I_1–I_2–I_3 three-spin system and (b) I_1–I_2–I_3–I_4 four-spin system. Displacement vectors (arrows with solid lines) $\mathbf{J}_i^{(12)} = (J_{1i}, J_{2i})$ are associated with each of the passive spins I_i. They connect basic squares with side lengths equal to the active coupling constant J_{12}. Arrows with broken lines are described in the text. The angle φ_i between $\mathbf{J}_i^{(12)}$ and the ω_2 axis reflects the relative sign of J_{1i} and J_{2i} (see text). In this figure $J_{13} \times J_{23} > 0$ and $J_{14} \times J_{24} < 0$. The abbreviation $s_i = \mathrm{sgn}(J_{1i} \cdot J_{2i})$ is used in (b).

displacement vector $\mathbf{J}_i^{(12)}$ reflects the sign of the product $J_{1i} \cdot J_{2i}$. φ_i can take all values between 0 and 2π, but because E.COSY spectra for weak coupling are invariant to selective inversions of displacement vectors $((J_{1i}, J_{2i}) \rightarrow (-J_{1i}, -J_{2i}))$ we draw displacement vectors such that only the range $0 < \varphi_i < \pi$ occurs. When the diagonal runs from the upper right to lower left in the spectrum, $0 < \varphi_i < \pi/2$ and $\pi/2 < \varphi_i < \pi$ are indicative of $J_{1i} \cdot J_{2i} > 0$ and $J_{1i} \cdot J_{2i} < 0$, respectively. With the restriction $0 < \varphi_i < \pi$ the components of a difference or sum vector between two displacement vectors (see Fig. 4b) are given by

$$\mathbf{J}_3^{(12)} \mp \mathbf{J}_4^{(12)} = (|J_{13}| \mp |J_{14}|, \operatorname{sgn}(J_{13} \cdot J_{23})|J_{23}| \mp \operatorname{sgn}(J_{14} \cdot J_{24})|J_{24}|). \quad [6]$$

Arrows with broken lines indicate linear combinations of displacement vectors with the active coupling constant J_{12}. Obviously, the addition of $(J_{12}, 0)$ or $(0, J_{12})$ to a displacement vector does not change the ω_2 or ω_1 components, respectively. These combined vectors are especially useful for extraction of J (vide infra). In the following experimental spectra, vectors are marked with the associated passive spins irrespective of the active coupling constants being included or not (see e.g. Fig. 5).

APPLICATION OF E.COSY TO THE ANALYSIS OF PEPTIDE SPIN SYSTEMS

Procedures for extraction and assignment of J values from E.COSY spectra are exemplified by experimental spectra of the cyclic decapeptide antamanide, cyclo(-Val[1]-Pro[2]-Pro[3]-Ala[4]-Phe[5]-Phe[6]-Pro[7]-Pro[8]-Phe[9]-Phe[10]-). A simplified notation is used to address the various protons: $\alpha = C_\alpha H$, $\beta_1 = C_\beta H_1$, etc.

NH–$C_\alpha H$ connectivities. The assignment of peptide and protein COSY spectra often starts with the NH-α connectivities. E.COSY opens the possibility for determination of four-bond $J_{NH\beta}$ couplings in amino acid residues. For illustration the $\alpha \rightarrow$ NH E.COSY cross-peak multiplet of Val[1] is shown in Fig. 5. (We employ a systematic notation in which $x \rightarrow y$ means the cross-peak multiplet with spins x and y active in the t_1 and t_2 periods, respectively. The notation x–y refers to both cross peaks $x \rightarrow y$

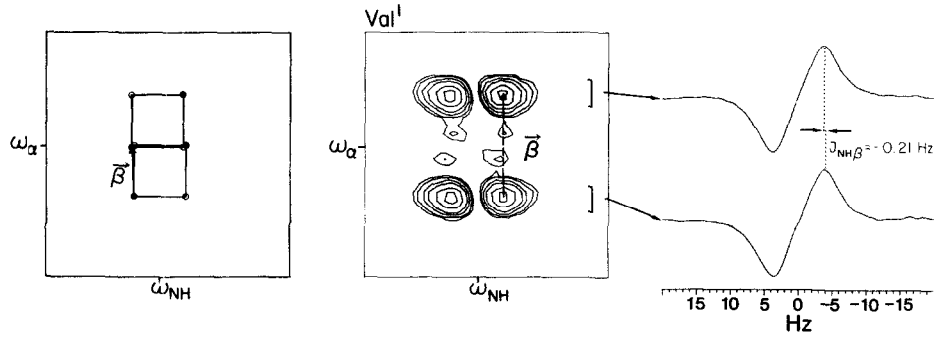

FIG. 5. The $\alpha \rightarrow$ NH E.COSY cross-peak multiplet of Val[1] in antamanide experimentally and schematically along with 1D traces appropriate for measurement of the four-bond $J_{NH\beta}$ coupling constant. Sections parallel to the ω_2 axis within the indicated brackets were coadded. In this and all following experimental spectra the contour levels are plotted at 90, 67.5, 45, 33.75, 22.5, and 16.875% of the highest peak in the excerpt shown. Furthermore, some 1D traces (here the upper one) are phase-inverted in order to ease comparison.

and $y \rightarrow x$.) The multiplet consists of two basic squares displaced by the $\mathbf{J}_{\beta}^{(\mathrm{NH}\alpha)}$ displacement vector as also depicted schematically in Fig. 5. The active coupling constant $J_{\mathrm{NH}\alpha}$ (7.2 Hz) is similar to the passive coupling constant $J_{\alpha\beta}$ (6.8 Hz) leading to cancellation in the center of the multiplet. $J_{\mathrm{NH}\beta}$ can be determined from 1D traces (on the right in Fig. 5) obtained by coadding sections parallel to the ω_2 axis (indicated by brackets). The coaddition improves the signal-to-noise ratio and the accuracy of the measurement. A mean value $J_{\mathrm{NH}\beta} = -0.21$ Hz with standard deviation 0.01 Hz could be determined from this cross peak and from six independent displacements of 1D traces in the $\alpha \rightarrow \beta$ cross-peak multiplet.

$C_\alpha H$–$C_\beta H$ connectivities. Figure 6 shows as an example of $C_\alpha H$–$C_\beta H$ connectivities the $\beta_1 \rightarrow \alpha$ multiplet of Phe[10]. For this NH$\alpha\beta_1\beta_2$ four-spin system, $2^{2 \cdot 4-2} = 64$ multiplet components are expected in the COSY $\beta_1 \rightarrow \alpha$ cross peak while in E.COSY only $2^4 = 16$ multiplet components occur. The interpretation is given schematically on the left in Fig. 6.

For determining $J_{\alpha\beta_2}$ it is best to compare sections parallel to ω_2 at the peripheral ω_1 positions in order to circumvent the partial overlap in the center. In principle $J_{\mathrm{NH}\alpha}$ could also be measured from Fig. 6 as a displacement of two peaks in ω_2. However, such a measurement would be no more accurate than a determination from the antiphase doublet in the $\alpha \rightarrow$ NH cross peak because the very small $^4J_{\mathrm{NH}\beta_1}$ does not provide any useful spread along ω_1 as shown in Fig. 6.

Coupling constants involving β_1 could be determined from the $\beta_1 \rightarrow \alpha$ cross peak in Fig. 6 as relative peak displacements in the ω_1 dimension. But due to the usually better resolution in ω_2, coupling constants should whenever possible be extracted from sections parallel to ω_2. $J_{\mathrm{NH}\beta_1}$ and $J_{\beta_1\beta_2}$ are therefore determined from the $\alpha \rightarrow \beta_1$ cross-peak multiplet situated at the position symmetric with respect to the diagonal (Fig. 7). The tiny $^4J_{\mathrm{NH}\beta_1} = -0.25$ Hz coupling constant can conveniently be measured from this cross-peak multiplet because the ω_1 component ($J_{\mathrm{NH}\alpha}$) is well-resolved.

The above examples illustrate a basic requirement for the measurement of J from E.COSY spectra: In order to determine J_{km} from an I_k–I_l cross peak, the other component J_{lm} of the $\mathbf{J}_m^{(kl)}$ displacement vector must be resolved. The following examples will show that measurement of the coupling constants associated with $\mathbf{J}_m^{(kl)}$ also requires the difference vectors $\mathbf{J}_m^{(kl)} - \mathbf{J}_n^{(kl)}$ between $\mathbf{J}_m^{(kl)}$ and all other displacement vectors

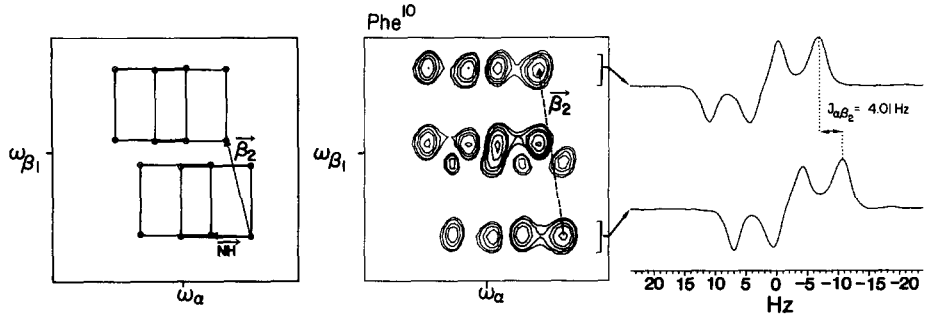

FIG. 6. The $\beta_1 \rightarrow \alpha$ E.COSY cross-peak multiplet of Phe[10] in antamanide experimentally and schematically along with 1D traces appropriate for measurement of the vicinal coupling constant $J_{\alpha\beta_2}$.

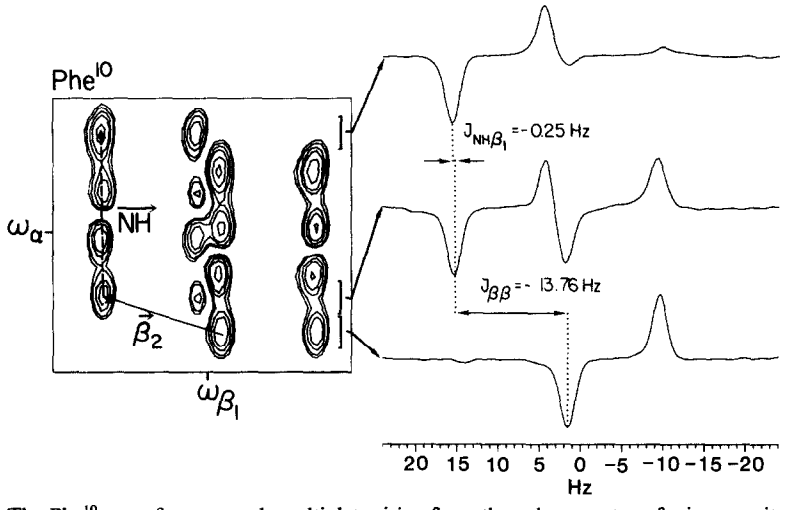

FIG. 7. The Phe[10] $\alpha \rightarrow \beta_1$ cross-peak multiplet arising from the coherence transfer in opposite direction to the one in Fig. 6. This cross peak is favorable for measuring the tiny four-bond $J_{NH\beta_1}$ coupling constant along the better resolved ω_2 axis.

$\mathbf{J}_n^{(kl)}$ to be resolved. In general also the difference vectors between $\mathbf{J}_m^{(kl)}$ and sums of other displacement vectors (e.g., $\mathbf{J}_m^{(kl)} - (\mathbf{J}_n^{(kl)} + \mathbf{J}_o^{(kl)})$) need to be resolved.

More complicated E.COSY multiplet patterns occur for β–α cross peaks when further spins couple to the β protons as encountered for example in proline residues. The $\beta_1 \rightarrow \alpha$ and $\beta_2 \rightarrow \alpha$ cross peaks of Pro[8] are shown in Figs. 8a and 8b, respectively. Four nonoverlapping basic squares are visible in Fig. 8a because the active coupling

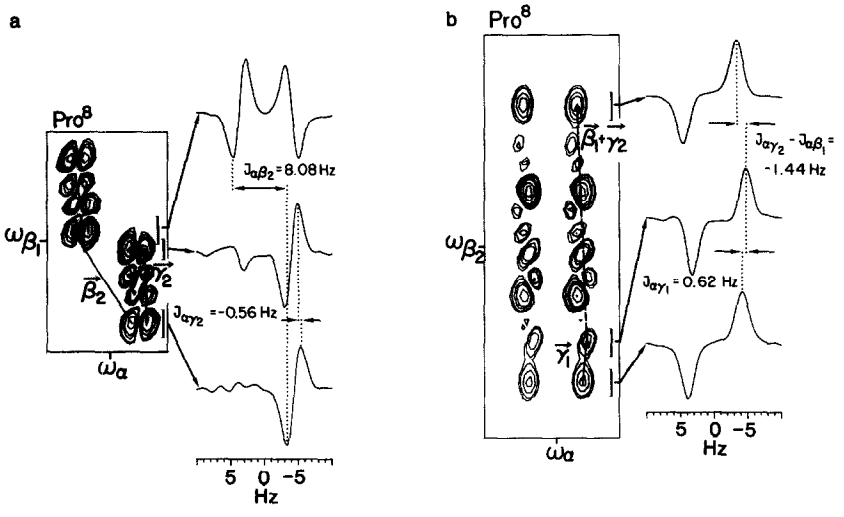

FIG. 8. Pro[8] $\beta_{1,2} \rightarrow \alpha$ cross peaks. Two facts are responsible for the much simpler pattern in (a) compared to (b): a small active coupling constant and fully resolved difference displacement vectors. The main complication in (b) is $\mathbf{J}_{\beta_1}^{(\beta_2\alpha)} \approx \mathbf{J}_{\gamma_2}^{(\beta_2\alpha)}$ which allows only the linear combination $\mathrm{sgn}(J_{\alpha\beta_1} \cdot J_{\beta_2\beta_1})|J_{\alpha\beta_1}| + \mathrm{sgn}(J_{\alpha\gamma_2} \cdot J_{\beta_2\gamma_2})|J_{\alpha\gamma_2}|$ to be determined.

$J_{\alpha\beta_1}$ is small (0.9 Hz). Of the two associated displacement vectors, $\mathbf{J}_{\beta_2}^{(\beta_1\alpha)}$ can be unambiguously assigned based on the large magnitude of geminal coupling constants. The other displacement vector has to be due to one of the γ protons. The distinction between γ_1 and γ_2 cannot be made from this cross peak alone but follows from the magnitudes of $J_{\beta_1\gamma_1}$ (1.4 Hz) and $J_{\beta_2\gamma_2}$ (6.5 Hz) which can be extracted from other E.COSY cross peaks.

The individual multiplet components in Fig. 8a have elliptic peak shapes. This is caused by the third unresolved displacement vector $\mathbf{J}_{\gamma_1}^{(\beta_1\alpha)}$ where both components, $J_{\beta_1\gamma_1} = 1.4$ Hz and $J_{\alpha\gamma_1} = 0.6$ Hz, are small. Consequently, these two coupling constants cannot be determined from the α–β_1 cross peaks. However, the relative sign $J_{\alpha\gamma_1} \cdot J_{\beta_1\gamma_1} > 0$ follows from the tilt direction of the elliptic peak shapes. In inhomogeneous static fields care must be taken that tilted elliptic peak shapes caused by coherence transfer echoes are not misinterpreted as unresolved long-range couplings.

The appearance of the $\beta_2 \rightarrow \alpha$ cross-peak multiplet in Fig. 8b is very different from the $\beta_1 \rightarrow \alpha$ multiplet in Fig. 8a and illustrates the situation with a vanishing difference between two displacement vectors. The pattern is characterized by three displacement vectors:

$$\mathbf{J}_{\beta_1}^{(\beta_2\alpha)} = (-12.5, 0.9)$$

$$\mathbf{J}_{\gamma_1}^{(\beta_2\alpha)} = (6.8, 0.6)$$

$$\mathbf{J}_{\gamma_2}^{(\beta_2\alpha)} = (13.0, -0.6).$$

According to Eq. [6] the difference vector between $\mathbf{J}_{\beta_1}^{(\beta_2\alpha)}$ and $\mathbf{J}_{\gamma_2}^{(\beta_2\alpha)}$ amounts to (0.5, −0.3) which is unresolved. In contrast, the displacement vector $\mathbf{J}_{\gamma_1}^{(\beta_2\alpha)}$ is well-resolved and $J_{\alpha\gamma_1}$ can be measured. The displacement of the upper two 1D spectra plotted in Fig. 8b is given by

$$\mathrm{sgn}(J_{\beta_2\beta_1} \cdot J_{\alpha\beta_1})|J_{\alpha\beta_1}| + \mathrm{sgn}(J_{\beta_2\gamma_2} \cdot J_{\alpha\gamma_2})|J_{\alpha\gamma_2}| = -1.44\,\mathrm{Hz}.$$

The examples shown in Fig. 8 illustrate that the analysis of an E.COSY cross peak often requires information gained from the analysis of other cross peaks.

CH_2–CH_2 fragments. The straightforward assignment of E.COSY vicinal cross-peak multiplet patterns arising from CH_2–CH fragments discussed in the previous section is due to the invariably large magnitude and the negative sign of geminal coupling constants. The same fact also simplifies the assignments in vicinal cross peaks of CH_2–CH_2 fragments:

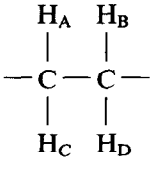

Consider by way of example the cross peak between H_A and H_B in a hypothetical four-spin system with the displacement vectors $\mathbf{J}_C^{(AB)}$ and $\mathbf{J}_D^{(AB)}$ as illustrated in Fig. 9. Vicinal coupling constants (here J_{AD} and J_{BC}) are usually positive and vary from 0 to 13 Hz where the upper limit extends into the range of the geminal J's. Their magnitudes are closely related to the torsional angle through the Karplus relation (*1–3*). However,

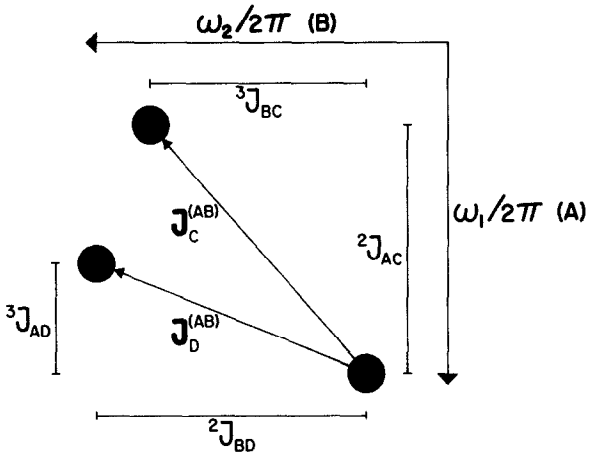

FIG. 9. Schematic diagram illustrating the basic feature of vicinal cross-peak multiplets in CH_2–CH_2 fragments (–C(H_AH_C)–C(H_BH_D)–). The indicated three peaks may be considered the lower right corners of three basic squares in the $H_A \rightarrow H_B$ cross-peak multiplet. As mentioned in the text, the smallest of the involved four coupling constants belongs to a three-bond coupling. The assignment of the remaining three coupling constants is then unambiguous.

there is no conformational arrangement where both vicinal coupling constants are as large as geminal coupling constants. Therefore the smallest of the four components of the two displacement vectors belongs always to a three-bond coupling. The other component of the same vector must then be a two-bond coupling constant. The opposite arrangement of ^2J and ^3J in the two dimensions applies for the second displacement vector.

As an example, the Pro[8] $\delta_1 \rightarrow \gamma_1$ E.COSY cross-peak multiplet is shown in Fig. 10. The two main displacement vectors $\mathbf{J}_{\delta_2}^{(\delta_1\gamma_1)}$ and $\mathbf{J}_{\gamma_2}^{(\delta_1\gamma_1)}$ are clearly seen, and the distinction between the two follows from the small component of $\mathbf{J}_{\delta_2}^{(\delta_1\gamma_1)}$ in the ω_2 dimension which is indicative of a vicinal coupling constant.

The $\gamma_2 \rightarrow \delta_2$ cross-peak multiplet of Pro[8] in Fig. 11 represents a CH_2–CH_2 extension of the $\beta_2 \rightarrow \alpha$ CH_2–CH pattern in Fig. 8b. The assignment of $\mathbf{J}_{\delta_1}^{(\gamma_2\delta_2)}$ is obvious because it is the only displacement vector with large components in both frequency dimensions. The difference vector of $\mathbf{J}_{\beta_2}^{(\gamma_2\delta_2)}$ and $\mathbf{J}_{\gamma_1}^{(\gamma_2\delta_2)}$ is not resolved, and only the linear combination

$$\mathrm{sgn}(J_{\gamma_2\beta_2}J_{\delta_2\beta_2})|J_{\beta_2\delta_2}| + \mathrm{sgn}(J_{\gamma_2\gamma_1}J_{\delta_2\gamma_1})|J_{\gamma_1\delta_2}| = -1.87\,\mathrm{Hz}$$

can be measured directly. The knowledge about $J_{\gamma_1\delta_2}$ from the $\delta_1 \rightarrow \gamma_1$ cross peak then allows the determination of $J_{\beta_2\delta_2}$.

A similar cross-peak multiplet $\beta_1 \rightarrow \gamma_2$ is shown in Fig. 12. The measurement of J is impeded by the similarity of three displacement vectors:

$$\mathbf{J}_{\gamma_1}^{(\beta_1\gamma_2)} = (1.4, -13.1)$$

$$\mathbf{J}_{\delta_1}^{(\beta_1\gamma_2)} = (-0.6, 10.9)$$

$$\mathbf{J}_{\delta_2}^{(\beta_1\gamma_2)} = (0.4, 8.8).$$

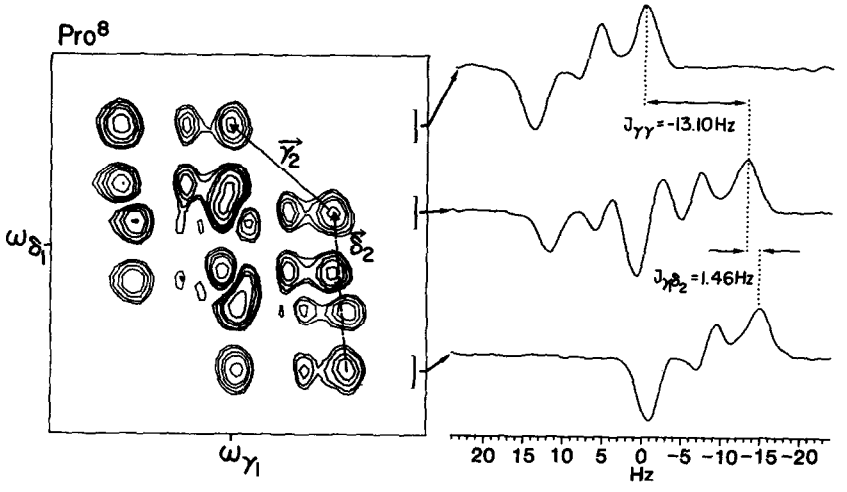

FIG. 10. Pro⁸ $\delta_1 \rightarrow \gamma_1$ cross peak illustrating the assignment in vicinal cross peaks. One of the four relevant coupling constants is clearly smaller than the others identifying it as the three-bond $J_{\gamma_1\delta_2}$.

The situation is made even worse by the small $\mathbf{J}_{\delta_2}^{(\beta_1\gamma_2)} = (0.9, -0.6)$ displacement vector. As a consequence the most intense peaks of the $\beta_1 \rightarrow \gamma_2$ multiplet consist of $3 \times 2 = 6$ overlapping peaks. Therefore only the vicinal $J_{\beta_2\gamma_2}$ coupling constant can be measured.

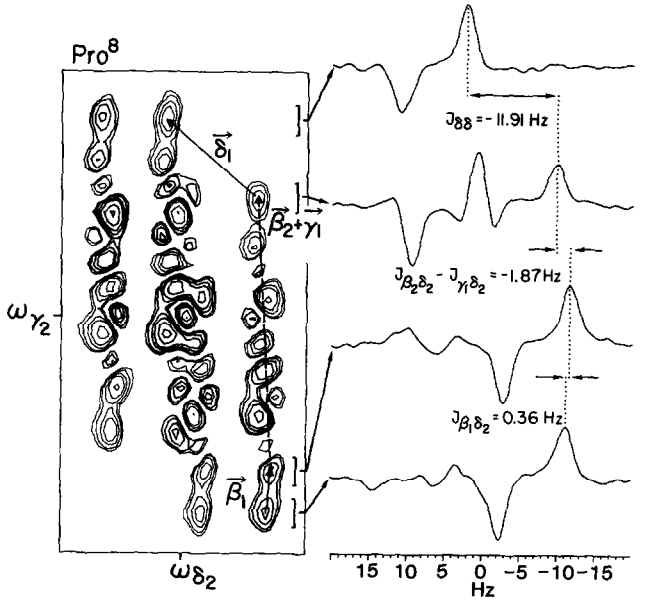

FIG. 11. Pro⁸ $\gamma_2 \rightarrow \delta_2$ cross-peak multiplet. Again the assignment of the two displacement vectors $\mathbf{J}_{\delta_1}^{(\gamma_2\delta_2)}$ and $\mathbf{J}_{\gamma_1}^{(\gamma_2\delta_2)}$ is unambiguous. The basic structure of this multiplet is similar to the $\beta_2 \rightarrow \alpha$ multiplet in Fig. 8b that is here duplicated by $\mathbf{J}_{\delta_1}^{(\gamma_2\beta_2)}$.

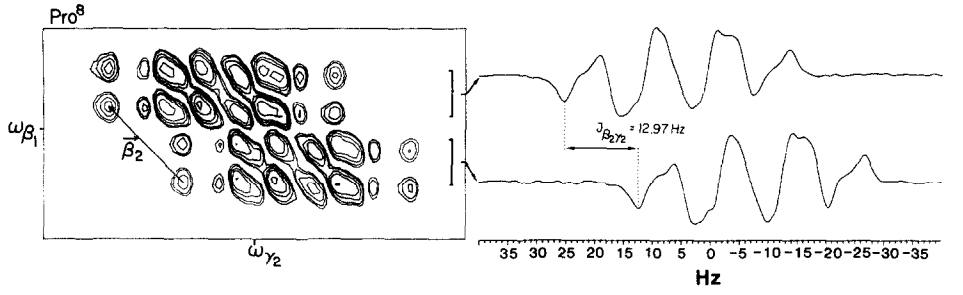

FIG. 12. Pro⁸ $\beta_1 \rightarrow \gamma_2$ cross-peak multiplet complicated by unresolved displacement and difference vectors (see text). The assignment of $\mathbf{J}_{\beta_2}^{(\beta_1\gamma_2)}$ follows the usual procedure.

The cross peaks with the largest number of relevant spins in proline residues arise from coherence transfer between β and γ protons; the $\beta_2 \rightarrow \gamma_2$ multiplet is shown in Fig. 13. Again the $\mathbf{J}_{\beta_1}^{(\beta_2\gamma_2)}$ and $\mathbf{J}_{\gamma_1}^{(\beta_2\gamma_2)}$ displacement vectors of the CH_2–CH_2 fragment can easily be localized. Also the assignment of $\mathbf{J}_{\alpha}^{(\beta_2\gamma_2)}$ is unambiguous due to its relatively large component in the ω_1 dimension. The difference vector between the two δ displacement vectors

$$\mathbf{J}_{\delta_1}^{(\beta_2\gamma_2)} = (0.0, 10.9)$$

$$\mathbf{J}_{\delta_2}^{(\beta_2\gamma_2)} = (-0.4, 8.8)$$

is, however, not resolved.

Geminal cross peaks. All the cross-peak multiplets discussed so far occur between vicinal protons. Strong E.COSY cross peaks are also observed between geminal protons.

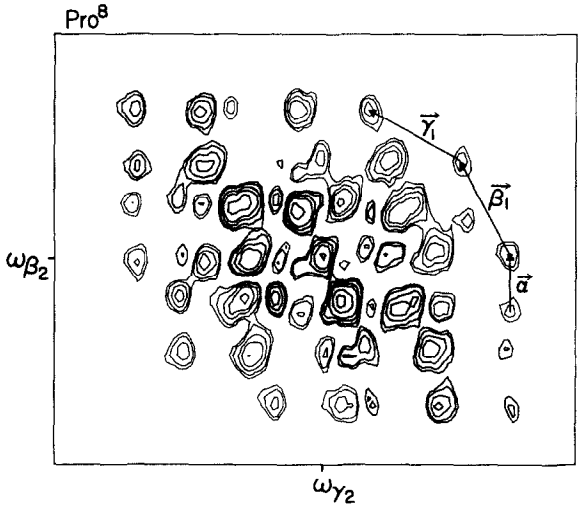

FIG. 13. Pro⁸ $\beta_2 \rightarrow \gamma_2$ cross-peak multiplet. The assignment of the two displacement vectors within the CH_2–CH_2 fragment causes no problems. The identification of $\mathbf{J}_{\alpha}^{(\beta_2\gamma_2)}$ follows from the relatively large component in the ω_1 dimension ($J_{\alpha\beta_2}$) which excludes the possibility of a four-bond coupling constant. However, the difference vector between $\mathbf{J}_{\delta_1}^{(\beta_2\gamma_2)}$ and $\mathbf{J}_{\delta_2}^{(\beta_2\gamma_2)}$ is not resolved.

However, the number of relevant passive spins for geminal cross peaks is usually larger than that for vicinal cross peaks, increasing the chance of overlap between displacement vectors. Furthermore, and most importantly for the assignment, there are no passive coupling constants of known value, such as $^2J_{HH}$ in vicinal multiplets, that would ease the assignment. In many cases, however, a complete determination of the coupling network is possible without taking recourse to a detailed analysis of the geminal cross peaks.

Usage of complementary E.COSY spectra. The complementary E.COSY spectrum contains, in principle, no information not present in the normal E.COSY spectrum. The complementary spectrum, which correlates anti-connected transitions (i.e., transitions with opposite polarization of all passive spins), is obtained in the weak coupling limit from the normal spectrum by replacing φ_i in the displacement vectors $\mathbf{J}_i^{(kl)}$ by $\pi - \varphi_i$. As an example, the Pro[8] $\gamma_2 \rightarrow \delta_1$ cross-peak multiplets in normal and complementary E.COSY are shown in Fig. 14. This figure demonstrates that the replacement of φ_i by $\pi - \varphi_i$ inherent in complementary E.COSY is equivalent to a reflection about a central plane verifying that normal and complementary E.COSY spectra contain the same information. It can, however, occur that unrelated cross-peak multiplets overlap in one of the two spectra and are resolved in the other.

SENSITIVITY AND SELECTION OF SCAN NUMBERS

In this section we discuss the selection of the numbers of scans NS_j for the individual experiments with phases β_j and the overall sensitivity of the experiment. The sensitivity of E.COSY is conveniently expressed relative to the sensitivity of 2QF COSY which is a well-established technique. We consider only the practically most relevant E.COSY version with the weights B_0 and B_1 of the zero- and single-quantum-filtered spectra set equal to zero which eliminates the net magnetization on the diagonal.

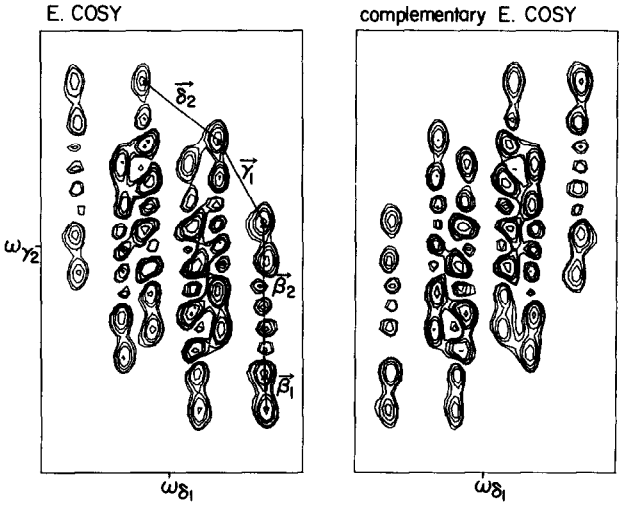

FIG. 14. Pro[8] $\gamma_2 \rightarrow \delta_1$ E.COSY and complementary E.COSY cross peaks. The two multiplets are related by a vertical or horizontal reflection.

It is a fact well-known in information theory that the optimum signal-to-noise ratio per unit time is obtained when experiments with the same noise variance are combined without numerical weighting. In the present context this implies that the E.COSY weighting factors W_j are taken into account by adjusting the number of scans NS_j for the phases β_j, i.e., $NS_j = k|W_j|$, where k is a constant for all j. It was shown in Ref. (*17*) that the relative sensitivity $\mathcal{S}$ (E.COSY compared to 2QF COSY) for a cross peak with K_c ($2 \leqslant K_c \leqslant K$) relevant spins is

$$\mathcal{S} = \begin{cases} \dfrac{2^{K_c}}{K^2 - 1} & \text{for } K \text{ odd} \quad [7a] \\ \dfrac{2^{K_c}}{K^2} & \text{for } K \text{ even,} \quad [7b] \end{cases}$$

where K is the highest quantum order employed in the E.COSY linear combination (see Eqs. [1] and [3]).

The relative sensitivity $\mathcal{S}$ in Eq. [7] is given for a nondegenerate multiplet component in the two spectra. Degeneracy of transitions or resonance overlap due to broad lines tends to enhance the sensitivity of 2QF COSY. This is illustrated in Fig. 15 with cross peaks from simulated 2QF COSY and E.COSY spectra of two different three-spin systems. For the cross peak in Fig. 15a there is equal intensity for 2QF COSY and E.COSY because all multiplet components are well separated. In Fig. 15b the overlaps, due to the small coupling, lead to a higher effective sensitivity in 2QF COSY than in E.COSY. This is a common situation in applications to biomolecules with short T_2 relaxation times.

It can be necessary for practical reasons to select the scan numbers $NS_j \neq k|W_j|$ and to introduce numerical weighting factors $|W_j|/NS_j$, for example, when the weights W_j are not convenient integers. This happens at the expense of sensitivity with the reduction factor R given by the expression

$$R = \frac{\sum_{j=0}^{2N-1} |W_j|}{\left\{\left[\sum_{j=0}^{2N-1} NS_j \left(\frac{W_j}{NS_j}\right)^2\right]\left[\sum_{j=0}^{2N-1} NS_j\right]\right\}^{1/2}} \quad [8]$$

in accordance with optimum sensitivity ($R = 1$) occurring for $NS_j = k|W_j|$.

Sometimes, it is of interest to record both the normal and the complementary E.COSY spectra, either because certain peaks may be resolved only in one of the two spectra or because some computer pattern recognition procedures (*18*) rely on both spectra. The two spectra can be constructed from the same data set by performing differently weighted linear combinations according to Eqs. [1] and [3]–[5]. This obviously renders impossible the fulfillment of the condition $NS_j = k|W_j|$ for both spectra. In order to obtain equal sensitivities for both spectra it is necessary to set equal the scan numbers of experiments that differ in phase by π, i.e., $NS_j = NS_{j+N}$. It is found that under this condition maximum sensitivity is obtained for

$$NS_j = k\sqrt{W_j^2 + W_{j+N}^2}. \quad [9]$$

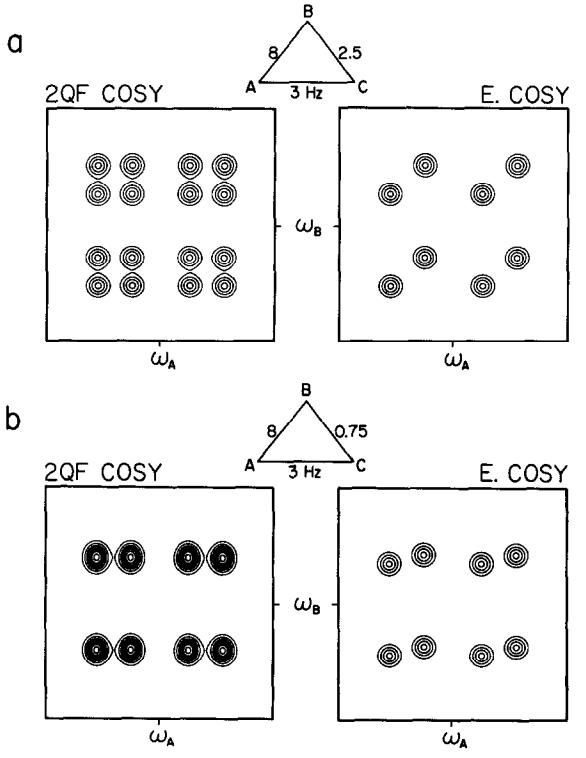

FIG. 15. Simulated 2QF COSY and E.COSY B → A cross-peak multiplets of two A–B–C three-spin systems in the weak coupling limit. The coupling constants are indicated in the triangular coupling networks. Gaussian lineshapes with linewidth 1.5 Hz at half height are assumed. (a) When all multiplet components are well-resolved the sensitivities of 2QF COSY and E.COSY are identical. (b) The unresolved J_{BC} coupling constant results in a higher effective sensitivity in 2QF COSY than in E.COSY. The $\alpha \rightarrow$ NH cross-peak multiplet in Fig. 5 is an extreme example of the case in (b) where E.COSY is associated with a sensitivity reduction of a factor 2 compared to 2QF COSY. The same equidistant contour levels are employed in all spectra; in the E.COSY spectrum of (a), they correspond to 92.8, 71.4, 50.0, and 28.6% of the peak intensities.

The resulting sensitivity reduction in comparison with an individually optimized experiment is tabulated in Table 2 for $2 \leq K = N \leq 8$. It ranges between 1 and $1/\sqrt{2}$, the latter value corresponding to separately recorded experiments.

The sensitivity loss experienced by the cross peaks with small K_c when K is large can become unacceptable. Some of the sensitivity can be recovered by separate storage of the individual experiments β_j, $j = 0, 1, \ldots, 2N-1$ followed by different linear combinations for several values of K (see Eq. [4]). Obviously, only cross peaks with a number of relevant spins $K_c \leq K$ will exhibit true E.COSY patterns.

The general expression for the sensitivity of E.COSY relative to 2QF COSY for a cross peak with K_c relevant spins is then conveniently written as a function of the three parameters N, K_c^0, and $K_c = K$:

$$\mathcal{S}(N, K_c^0, K_c) = \frac{N \cdot 2^{K_c-2}}{\{(\sum_{j=0}^{2N-1} W_j^2(K_c)/\mathrm{NS}_j(K_c^0))(\sum_{j=0}^{2N-1} \mathrm{NS}_j(K_c^0))\}^{1/2}}, \qquad K_c^0, K_c \leq N. \quad [10]$$

TABLE 2

Sensitivity Reduction Factor R for an E.COSY Experiment Simultaneously Optimized for Normal and Complementary E.COSY Relative to an Experiment Optimized for One of the Spectra Only

$N = K$	2	3	4	5	6	7	8
R	1.00	0.82	0.84	0.78	0.79	0.76	0.76

The value of N determines the increment (π/N) in the phase cycle, the scan numbers are optimized for K_c^0 ($NS_j = W_j(K_c^0)$), and the E.COSY linear combination employs $K = K_c$. This function has been tabulated in Table 3 for $3 \leq N, K_c^0, K_c \leq 6$. The table makes clear that separate storage of the individual phase-shifted experiments and careful consideration of the scan numbers are worthwhile in cases of critical sensitivity. For a $2N$-step phase cycle this amounts to separate storage of $N + 1$ 2D files; $2N - 2$ of the files can be combined pairwise because of the symmetry

TABLE 3

Sensitivity of E.COSY Relative to 2QF COSY as a Function of N, K_c°, K_c (See Text) for a Cross Peak with K_c Relevant Spins

N	K_c \ K_c°	3	4	5	6
3	3	1 (1)			
4	3	0.69 (1.37)	0.56 (1.12)		
	4	0.88 (0.88)	1 (1)		
5	3	0.77 (2.32)	0.52 (1.57)	—	
	4	0.49 (0.73)	0.71 (1.06)	—	
	5	0.62 (0.47)	1.12 (0.84)	1.33 (1)	
6	3	0.75 (3.38)	0.55 (2.49)	0.49 (2.19)	0.47 (2.13)
	4	0.68 (1.53)	0.75 (1.69)	0.51 (1.15)	0.51 (1.15)
	5	0.66 (0.74)	0.67 (0.75)	0.91 (1.02)	0.67 (0.75)
	6	0.96 (0.54)	1.14 (0.64)	1.51 (0.85)	1.78 (1)

Note. The numbers in parentheses are E.COSY sensitivities relative to the E.COSY spectrum employing $K_c^\circ = K_c^{max}$ equal to N.

$$W_j = W_{2N-j}, \qquad j \neq N. \qquad [11]$$

Note that Eq. [9] should also be observed when both the normal and the complementary E.COSY spectra are desired.

APPROXIMATE E.COSY SPECTRA

In this section, we describe simplified approaches that generate approximate E.COSY spectra. By approximate is meant that the cross-peak multiplet components corresponding to correlation between nonconnected transitions are not completely suppressed. In some cases such small residual artifacts may be tolerable.

It is known that a small flip-angle COSY experiment with the sequence 90°_x–t_1–β_y–t_2 enhances cross peaks corresponding to connected transitions relative to those of nonconnected transitions (*8, 9*). The intensity ratio of the desired and the most intense undesired multiplet components is $\tan^2(\beta/2)$. A drawback of this experiment is the occurrence of huge diagonal peaks for small β which can obscure nearby cross peaks. This problem can be alleviated by subtracting an experiment with $\beta = 0$ which leads to elimination of the net dispersive magnetization on the diagonal. In this "compensation experiment" a "mixing delay" equal to the length of the β pulse should be included. The analogous version of β-COSY corresponding to complementary E.COSY subtractively combines experiments with β close to 180° and $\beta = 180°$.

Incomplete linear combinations, i.e., $K \leqslant K_c^{\max}$, result in E.COSY patterns for the cross peaks with $K_c \leqslant K$, but only approximate E.COSY patterns for those with $K_c > K$. The sensitivity of this approach is higher than that for $K = K_c^{\max}$ because of K^2 in the denominator in Eq. [7]. The relative residual amplitudes for the range $3 \leqslant K$, $K_c \leqslant 8$ have been tabulated in Table 4. We typically employ $N = K = 4$ when recording E.COSY spectra of peptides.

DISCUSSION

E.COSY has turned out to be a powerful technique for the extraction of scalar coupling constants from 2D spectra of complicated molecules. It is particularly useful for the analysis of spin coupling networks in peptides. The known magnitude of the geminal couplings usually allows a straightforward assignment of individual couplings. Many long-range couplings can be measured that are not accessible by other techniques.

TABLE 4

Amplitudes of Undesired Relative to Desired Multiplet Components in Incomplete E.COSY Linear Combinations

K \ K_c	3	4	5	6	7	8
3	0	0.23	0.30	0.32	0.33	0.33
4		0	0.07	0.11	0.14	0.15
5			0	0.02	0.04	0.06
6				0	0.01	0.01
7					0	0.00
8						0

As an example, we give in Table 5 the coupling constants for six amino acid residues in antamanide. They have been measured from displacements along ω_2 in an E.COSY spectrum with $N = K = 4$. The data matrix, consisting of 1500 points in the t_1 dimension and 4K points in t_2, was zero-filled to 4K × 8K points prior to the 2D Fourier transformation. In order to improve the digital resolution for measurements of J, the selected 1D traces were inverse Fourier transformed, zero-filled to 32K points, and Fourier transformed again. The standard deviations obtained from a set of independent measurements (either from different traces within a cross-peak multiplet or from different multiplets) indicate that the J values can be determined with high accuracy. Even coupling constants below 0.1 Hz can be measured without difficulty. In general, no cross peaks are observed between spins showing such small coupling constants. Numerous four-bond couplings are contained in Table 5, in particular NH–C_βH, C_αH–C_γH, and C_βH–C_δH couplings, in which both positive and negative signs have been found. The knowledge of accurate coupling constants may be helpful in determining side chain conformations of individual amino acid residues.

We should note that the strategy for extraction of coupling constants developed for

TABLE 5

Mean J Values (Hz) in Antamanide Measured from an E.COSY Spectrum

Phe[5]:	J(NH, β_1) = +0.15 ± 0.01 (4)	$J(\alpha\gamma_1)$ = +0.62 ± 0.02 (4)
	J(NH, β_2) = −0.32 ± 0.01 (4)	$J(\alpha\gamma_2)$ = −0.56 ± 0.02 (4)
	$J(\beta\beta)$ = −13.58 ± 0.03 (8)	$J(\beta\beta)$ = −12.48 ± 0.05 (18)
	$J(\alpha\beta_1)$ = +6.63 ± 0.06 (3)	$J(\beta_1\gamma_1)$ = +1.38 ± 0.10 (7)
	$J(\alpha\beta_2)$ = +7.96 ± 0.02 (2)	$J(\beta_1\gamma_2)$ = +6.42 ± 0.07 (9)
	J(NH, α) = +6.81	$J(\beta_1\delta_1)$ = −0.56 ± 0.06 (14)
Phe[6]:	J(NH, β_1) = −0.05 ± 0.02 (3)	$J(\beta_1\delta_2)$ = +0.36 ± 0.07 (6)
	J(NH, β_2) = −0.12 ± 0.01 (3)	$J(\beta_2\gamma_1)$ = +6.83 ± 0.01 (9)
	$J(\beta\beta)$ = −14.19 ± 0.01 (6)	$J(\beta_2\gamma_2)$ = +12.97 ± 0.04 (4)
	$J(\alpha\beta_1)$ = +5.83 ± 0.01 (2)	$J(\beta_2\delta_1)$ = −0.02 ± 0.06 (6)
	$J(\alpha\beta_2)$ = +5.68 ± 0.01 (2)	$J(\beta_2\delta_2)$ = −0.41 ± 0.02 (4)
	J(NH, α) = +6.62	$J(\gamma\gamma)$ = −13.10 ± 0.06 (11)
		$J(\gamma_1\delta_1)$ = +7.34 ± 0.06 (12)
Phe[9]:	J(NH, β_1) = −0.29 ± 0.02 (3)	$J(\gamma_1\delta_2)$ = +1.46 ± 0.09 (6)
	J(NH, β_2) = −0.08 ± 0.02 (3)	$J(\gamma_2\delta_1)$ = +10.88 ± 0.09 (6)
	$J(\beta\beta)$ = −14.04 ± 0.05 (4)	$J(\gamma_2\delta_2)$ = +8.81 ± 0.09 (9)
	$J(\alpha\beta_1)$ = +4.08 ± 0.01 (2)	$J(\delta\delta)$ = −11.91 ± 0.04 (11)
	$J(\alpha\beta_2)$ = +12.56 ± 0.02 (2)	
	J(NH, α) = +8.32	
		Pro[3]: $J(\alpha\beta_1)$ = +1.91 ± 0.05 (4)
Phe[10]:	J(NH, β_1) = −0.25 ± 0.01 (2)	$J(\alpha\beta_2)$ = +8.50 ± 0.06 (4)
	J(NH, β_2) = +0.19 ± 0.01 (4)	$J(\alpha\gamma_1)$ = +0.27 ± 0.04 (4)
	$J(\beta\beta)$ = −13.76 ± 0.01 (6)	$J(\alpha\gamma_2)$ = −0.09 ± 0.04 (4)
	$J(\alpha\beta_1)$ = +11.10 ± 0.03 (4)	$J(\beta\beta)$ = −12.85 ± 0.05 (2)
	$J(\alpha\beta_2)$ = +4.01 ± 0.05 (4)	$J(\beta_1\gamma_1)$ = +2.15 ± 0.09 (2)
	J(NH, α) = +6.7	$J(\beta_1\gamma_2)$ = +6.46 (1)
Pro[8]:	$J(\alpha\beta_1)$ = +0.88 ± 0.03 (5)	$J(\beta_2\gamma_1)$ = +6.84 ± 0.08 (4)
	$J(\alpha\beta_2)$ = +8.08 ± 0.01 (4)	$J(\beta_2\gamma_2)$ = +11.93 (1)

Note. The standard deviations of the means are indicated with the number of independent measurements in parentheses. The J(NH, α) couplings are reproduced from Ref. (*15*).

E.COSY in this paper applies equally well to the experiments described in Refs. (*19*) and (*20*) that yield approximate E.COSY cross-peak patterns.

So far the theory of E.COSY (*17*) has been restricted to weak coupling between the nuclear spins. Likewise, the extraction of the J values in the preceding section assumed first-order spectra, a fact that obviously is not always fulfilled. Distortions of peak amplitudes in cross-peak multiplets are a common phenomenon in E.COSY spectra. However, because resonance frequencies are affected only in second order, the separation of peaks is frequently still a good measure for the coupling constants. In some cases it can be necessary to apply iterative computer fitting of E.COSY multiplets starting with parameters determined by a first-order analysis. Extremely strong coupling can lead to complicated phase- and amplitude-distorted multiplets which are more difficult to analyze.

ACKNOWLEDGMENTS

This research has been supported by the Swiss National Science Foundation. The sample of antamanide was provided by Dr. A. Müller and Professor H. Kessler, Frankfurt, and the simulated spectra in Fig. 15 were obtained by the program SMART developed by Dr. W. Studer (*21*). The manuscript has been edited by Mrs. I. Müller.

REFERENCES

1. M. KARPLUS, *J. Chem. Phys.* **30,** 11 (1959).
2. M. KARPLUS, *J. Am. Chem. Soc.* **85,** 2870 (1963).
3. V. F. BYSTROV, *Prog. Spectrosc.* **10,** 41 (1976).
4. R. R. ERNST, G. BODENHAUSEN, AND A. WOKAUN, "Principles of Nuclear Magnetic Resonance in One and Two Dimensions," Clarendon Press, Oxford, 1987.
5. K. WÜTHRICH, "NMR of Proteins and Nucleic Acids," Wiley–Interscience, New York, 1986.
6. W. P. AUE, J. KARHAN, AND R. R. ERNST, *J. Chem. Phys.* **64,** 4266 (1976).
7. G. WIDER, R. BAUMANN, K. NAGAYAMA, R. R. ERNST, AND K. WÜTHRICH, *J. Magn. Reson.* **42,** 73 (1981).
8. W. P. AUE, E. BARTHOLDI, AND R. R. ERNST, *J. Chem. Phys.* **64,** 2229 (1976).
9. A. BAX AND R. FREEMAN, *J. Magn. Reson.* **44,** 542 (1981).
10. U. PIANTINI, O. W. SØRENSEN, AND R. R. ERNST, *J. Am. Chem. Soc.* **104,** 6800 (1982).
11. A. J. SHAKA AND R. FREEMAN, *J. Magn. Reson.* **51,** 169 (1983).
12. M. RANCE, O. W. SØRENSEN, G. BODENHAUSEN, G. WAGNER, R. R. ERNST, AND K. WÜTHRICH, *Biochem. Biophys. Res. Commun.* **117,** 479 (1983).
13. D. MARION AND K. WÜTHRICH, *Biochem. Biophys. Res. Commun.* **113,** 967 (1983).
14. H. OSCHKINAT AND R. FREEMAN, *J. Magn. Reson.* **60,** 164 (1984).
15. H. KESSLER, A. MÜLLER, AND H. OSCHKINAT, *Magn. Reson. Chem.* **23,** 844 (1985).
16. C. GRIESINGER, O. W. SØRENSEN, AND R. R. ERNST, *J. Am. Chem. Soc.* **107,** 6394 (1985).
17. C. GRIESINGER, O. W. SØRENSEN, AND R. R. ERNST, *J. Chem. Phys.* **85,** 6387 (1986).
18. P. PFÄNDLER, G. BODENHAUSEEN, B. U. MEIER, AND R. R. ERNST, *Anal. Chem.* **57,** 2510 (1985).
19. H. OSCHKINAT, A. PASTORE, P. PFÄNDLER, AND G. BODENHAUSEN, *J. Magn. Reson.* **69,** 559 (1986).
20. L. MÜLLER, *J. Magn. Reson.* **72,** 191 (1987).
21. W. STUDER, *J. Magn. Reson.*, in press.